Research Article

Abdulwahab S. Almusallam*, Isameldeen E. Daffallah, and Lazhar Benyahia

Modeling the Deformation of Shear Thinning Droplets Suspended in a Newtonian Fluid

https://doi.org/10.1515/arh-2020-0113
Received Oct 16, 2020; accepted Dec 28, 2020

Abstract: In this work, we carried out numerical modeling of the large deformation of a shear thinning droplet suspended in a Newtonian matrix using the constrained volume model. The adopted approach was to consider making incremental corrections to the evolution of the droplet anisotropy equation in order to capture the experimental behavior of a shear thinning droplet when subjected to deformation due to imposed flow. The constrained volume model was modified by using different models to describe the viscosity of droplet phase: the Bautista *et al.* model, the Carreau-Yasuda model and the Power-law model. We found that by combining the constrained volume model with a simple shear thinning viscosity model we were able to describe the available experimental data for large deformation of a shear thinning droplet suspended in a Newtonian matrix. Moreover, we developed an equation approximating flow strength during droplet retraction, and we found that the model can accurately describe the experimental data of the retraction of a shear thinning droplet.

Keywords: Constitutive Modeling; shear thinning; Droplet deformation

1 Introduction

The modeling of polymer blends composed of Newtonian fluids have been extensively investigated by researchers [1–8], and their flow behavior—to a great extent—is well understood. On the other hand, the behavior of blends composed of non-Newtonian components remains a subject that needs further development. As an example of the complexity of the topic of blends composed of non-Newtonian components, consider the work of Greco [9]. Greco [9] has derived a small deformation model based on second order fluid model, where a second order fluid is one with constant viscosity, but its stress is also affected by the presence of the first and second normal stress coefficients. As a result of the complication in the expression of the constitutive equation that describes each phase comprising the blend, the theory that was developed by Greco to describe the effect of second order fluid is mathematically tedious. And, while the behavior of a Newtonian droplet in a Newtonian matrix is controlled by two parameters, namely the capillary number (Ca) and viscosity ratio, the Non-Newtonian droplet in a non-Newtonian matrix, according to the Greco's theory, is controlled by four more additional parameters: two Deborah numbers and two ratios of the two normal stress differences for both the matrix and the droplet phases.

The previously mentioned model and other models that have tackled the subject of blends composed of viscoelastic components assume that blends are mainly composed from Boger fluids, which are fluids that have a constant viscosity and significant normal stresses [10], and those models were limited to small deformation [9, 11–13]. Large deformation of droplets for such case has been modeled only by a few researchers [14–16] and numerically simulated by [17–19].

For the case of one or both of the phases composed from shear thinning components, only very few experimental studies exist for the effect of shear thinning on the deformation of a single droplet. Elmendorp and Maalcke [20] investigated a variety of combinations of droplet and matrix phase fluids, including moderately shear thinning droplets in a Newtonian matrix and the opposite setup. Both systems were studied at small droplet deformation conditions. Delaby *et al.* [21] carried out experimental work on non-Newtonian droplets suspended in a non-Newtonian matrix. The system was subjected to a uniaxial extensional flow, and droplet lengths as they extend in extensional flow were compared to droplet lengths assuming affine deformation. It was found that when droplet deformation was predicted using an extensional rate inside the droplet that is defined using a self-consistent approach, very good agreement with

***Corresponding Author: Abdulwahab S. Almusallam:** Department of Chemical Engineering, Kuwait University, P.O. Box 5969, Safat 13060, Kuwait; Email: Abdulwahab.almusallam@ku.edu.kw
Isameldeen E. Daffallah: Department of Chemical Engineering, Kuwait University, P.O. Box 5969, Safat 13060, Kuwait
Lazhar Benyahia: Institut des Molécules et Matériaux du Mans, UMR CNRS 6283, Université du Maine, 1 Avenue Olivier Messiaen, 72085 Le Mans, France

Open Access. © 2020 A. S. Almusallam *et al.*, published by De Gruyter. CC BY This work is licensed under the Creative Commons Attribution 4.0 License

experimental data was obtained. Their analytical work was carried out based on small deformation theory and it assumed a linear relationship between droplet length during extensional flow and the affine droplet length. Another study was done by Boufarguine *et al.* [22]. This study used a strongly shear thinning fluid as a droplet phase and subjected the shear thinning droplet to large shearing deformation. The droplet deformation was studied in addition to droplet retraction after stopping the flow. Interestingly, due to the strong shear thinning nature of the droplet fluid, the droplet, after being extended in shearing flow, stops its retraction after a short while from stopping the flow.

Some researchers have also explored the topic of a shear thinning fluid in a Newtonian matrix theoretically. Favelukis *et al.* [23] theoretically studied the deformation of a shear thinning single droplet suspended in a Newtonian matrix during uniaxial extensional flow. Harvie *et al.* [24] studied a shear thinning droplet suspended in a Newtonian liquid as it flows in a microchannel. They found that the shear thinning droplet phase can be replaced by another fluid whose viscosity is the average viscosity of the shear thinning fluid while it is within the contraction. Giraldo *et al.* [25] used the boundary element method to study the behavior of a shear thinning non-Newtonian droplet in a Newtonian matrix in a Couette flow. A non-Newtonian droplet deformed more than a Newtonian droplet with the same zero-shear viscosity. Peters *et al.* [6] have developed a constitutive equation for polymer blends based on the microstructural evolution of the anisotropy tensor, and derived a constitutive equation to describe stresses for blends with unequal viscosity between matrix and droplet phases. Later on, the Peters *et al.* model was compared to the rheology of blends composed of viscoelastic components by taking the viscosity to be obtained through the Carreau-Yasuda model [26]. The approach used by Peters *et al.* in their original work was to model the blend's microstructure by assuming passive mixing, *i.e.*, the droplet deforms passively with the imposed flow, and hence the droplet phase deformation is independent of the viscosity ratio between the droplet and matrix phases. Therefore, in their model, the microstructure is not affected by the viscosity ratio value, although the stress is affected.

In this work, we will attempt to describe the shear thinning behavior and incorporate it in the constrained volume droplet model by implementing an approach similar to that of Tyagi *et al.* [26] However, the rate of deformation inside the droplet will be used to evaluate the viscosity of the droplet phase through the three different models that will be coupled with the constrained volume model. The first is the Carreau-Yasuda model, which is a steady state model that relates viscosity to applied deformation. The second is the Bautista *et al.* model [27], which describes shear thinning fluids through a constitutive equation. The third is a simple power law model. Then, we will compare predictions to experimental results of Boufarguine *et al.* [22] for shearing flow and to Delaby's results for extensional flow. To our knowledge, there are no previous studies that couple a shear thinning constitutive model to a droplet model. Although droplet elasticity can play a role in large deformation shearing flow taking place at high flow rates, this topic is outside the scope of this current work.

2 Theoretical Background

2.1 The Constrained Volume Model

The following equation describes the average velocity gradient tensor ($\kappa^{\star}_{\alpha\beta}$) inside the droplet using the theory of Wetzel and Tucker [1]:

$$\kappa^{\star}_{\alpha\beta} = \Omega_{\alpha\beta} + \left(B_{\alpha\beta\kappa\lambda} + C_{\alpha\beta\kappa\lambda}\right) D_{\kappa\lambda}. \tag{1}$$

Note that we use the Einstein notation for vectors and tensors in this equation and all subsequent equations. $D_{\alpha\beta}$ is the applied rate of deformation tensor, $\Omega_{\alpha\beta}$ is the applied vorticity tensor, and $B_{\alpha\beta\kappa\lambda}$ and $C_{\alpha\beta\kappa\lambda}$ are the strain rate and vorticity fourth order concentration tensors, respectively. Those fourth order concentration tensors depend only on droplet anisotropy ($\hat{q}_{\alpha\beta} = \frac{1}{V_d}\int n_\alpha n_\beta dS$, where n_α is a unit vector normal to the interface of the droplet and S is the droplet surface area) and viscosity ratio ($M = \eta^{\star}/\eta$) between the blend's components [28, 29], where η is the viscosity of the matrix phase, $\eta^{\star}$ is the viscosity of the minor phase. The procedure for obtaining $B_{\alpha\beta\kappa\lambda}$ and $C_{\alpha\beta\kappa\lambda}$ from droplet anisoropy and viscosity ratio is detailed in Appendix A. Droplet anisotropy evolves according to the assumption that changes due to its interfacial retraction and due to convective applied flow are decoupled [30].

$$\left.\frac{d}{dt}\hat{q}_{\alpha\beta}(t)\right|_{total} = \left.\frac{d}{dt}\hat{q}_{\alpha\beta}(t)\right|_{convection} + \left.\frac{d}{dt}\hat{q}_{\alpha\beta}(t)\right|_{retraction} \tag{2}$$

where t is time. The droplet convection and retraction terms are described by the following two equations [31]:

$$\left.\frac{d}{dt}\hat{q}_{\alpha\beta}(t)\right|_{convection} = -\hat{q}_{\alpha\gamma}\kappa^{\star}_{\gamma\beta} - \hat{q}_{\beta\gamma}\kappa^{\star}_{\gamma\alpha} + \hat{q}_{\alpha\beta\kappa\lambda}\kappa^{\star}_{\kappa\lambda}, \tag{3}$$

$$\left.\frac{d}{dt}\hat{q}_{\alpha\beta}(t)\right|_{retraction} = -f(M,\phi)\frac{\Gamma}{\eta}V_a^{1/6}\hat{q}_{\alpha\gamma}^{3/2}\left[\hat{q}_{\gamma\beta}\right. \tag{4}$$

$$-\delta_{\gamma\beta} g\left(\hat{q}_{\alpha\beta}\right)\Big],$$

where Γ is the interfacial tension, V_a is the approximate volume of the ellipsoidal droplet which is expressed in the model in terms of invariants of the anisotropy tensor [4], $\delta_{\alpha\beta}$ is the identity tensor, $g\left(\hat{q}_{\alpha\beta}\right)$ is a function that is introduced in order to maintain constancy of droplet volume in the droplet retraction expression [4]. $\hat{q}_{\alpha\beta\kappa\lambda}$ is the fourth order anisotropy tensor, which is related to the second order anisotropy tensor via a closure described elsewhere [4]. $f(M, \phi)$ is a function of the viscosity ratio M and the volume fraction of the dispersed phase (ϕ):

$$f(M,\phi) = \frac{160c\left(27+30\sqrt{3}\right)^{\frac{1}{12}}(1+M)^2}{(16+19M)\left[8M^2+5M(4+19\phi)+4(3+20\phi)\right]} \tag{5}$$

where c is a constant with a value of 0.695. For the evolution of the shape of a single droplet, ϕ is given a value of zero. The viscosity of the major phase is assumed to follow Newtonian behavior, whereas for the minor phase, viscosity is evaluated at the magnitude of the rate of deformation tensor inside the droplet together with the model describing the shear thinning behavior of the droplet phase, and hence $\eta^\star$ is a value that changes during the deformation of the droplet.

2.2 Modeling Shear Thinning Behavior of Droplet Phase

The Carreau-Yasuda model is a simple model describing the steady state viscosity of a shear thinning fluid:

$$\frac{\eta^\star - \eta^\star_\infty}{\eta^\star_o - \eta^\star_\infty} = \left[1+\left(\tau_{CY}\,\dot{\gamma}^\star\right)^a\right]^{(n-1)/a} \tag{6}$$

where $\eta^\star_\infty$ is the viscosity at infinite shear rate, $\eta^\star_o$ is the zero-shear rate viscosity and τ_{CY}, a and n are considered to be fitting parameters. In order to have a frame-invariant equation, $\dot{\gamma}^\star$ is replaced by $\sqrt{2\left|D^\star_{\alpha\beta}D^\star_{\alpha\beta}\right|}$ where $D^\star_{\alpha\beta}$ the rate of deformation tensor inside the droplet.

Constitutive models exist for describing stresses and viscosity of shear thinning fluids such as micellar solutions. One of the constitutive models that are developed for predicting stresses in micellar solutions is the Bautista *et al.* model [27]. Examples of other constitutive models for micellar solutions are the Johnson Segalman model [32, 33], the modified Johnson Segalman model [34] and the Vasquez, McKinley and Cook model [35]. The Bautista model is capable of accurately describing shear thinning behavior of micellar solutions, in addition to the time dependent behavior of the viscosity, unlike the Carreau-Yasuda model, which provides no time-dependent behavior for the viscosity.

The Bautista *et al.* family of constitutive models consist of two parts: an equation describing fluidity through a Fredrickson model for fluidity, and a constitutive equation describing stress evolution. Having an equation describing stress and another describing a structure parameter (fluidity is an example of a structure parameter) is a commonly used technique in describing thixotropic fluids [36]. The original Bautista model [27] uses the Maxwell model for stress tensor evolution, although later publications used other types of constitutive models such as the Oldroyd-B model [37]. Boek *et al.* [38] have modified the Oldroyd-B Bautista model, since extensional viscosity predictions of the original Bautista model showed instability at large extensional flow rate values. Such model is later known as the MBM model and was used by later researchers to describe flow of micellar solutions in a circular axisymmetric capillary channel [39, 40]. In this work, we will use the original Bautista *et al.* model since the flow type developing inside the droplet that we will investigate in this work is predominantly shearing type.

The Bautista *et al.* model consists of an equation for stress evolution, which is that of the upper convected Maxwell equation:

$$\sigma^\star_{\alpha\beta} + \frac{\eta^\star}{G_o}\overset{\triangledown}{\sigma}{}^\star_{\alpha\beta} = 2\eta^\star D^\star_{\alpha\beta} \tag{7}$$

coupled to a fluidity equation by Fredrickson [41], where fluidity $\equiv \eta^{-1}$:

$$\frac{d\eta^{\star-1}}{dt} = \frac{1}{\tau_B}\left(\frac{1}{\eta^\star_o}-\frac{1}{\eta^\star}\right) + k\left(\frac{1}{\eta^\star_\infty}-\frac{1}{\eta^\star}\right)\sigma^\star_{\alpha\beta}D^\star_{\alpha\beta} \tag{8}$$

The last term in the above equation has been proven and validated by Stephanou *et al.* [42] and Stephanou [43]. $\sigma^\star_{\alpha\beta}$ is the stress value of the droplet phase, G_o is the elastic modulus, τ_B is the relaxation time of the Bautista model, and k is a structural relaxation parameter of the droplet phase. The latter parameter is taken to be a constant in this work, although other publications have assumed that k is dependent on flow strength [39]. The symbol $\triangledown$ placed on top of the stress tensor denotes the upper convected derivative. Thus, $\sigma^\star_{\alpha\beta}$ and $\eta^\star$ are updated according to the value of $D^\star_{\alpha\beta}$ in the constrained volume model.

It is important at this point to note that all the modeling approaches for a shear thinning fluid that we implemented in this work will alter the microstructure evolution in the CV model, because the microstructural evolution depends on viscosity ratio, and because the velocity gradient inside the droplet depends on the viscosity ratio as well. Since

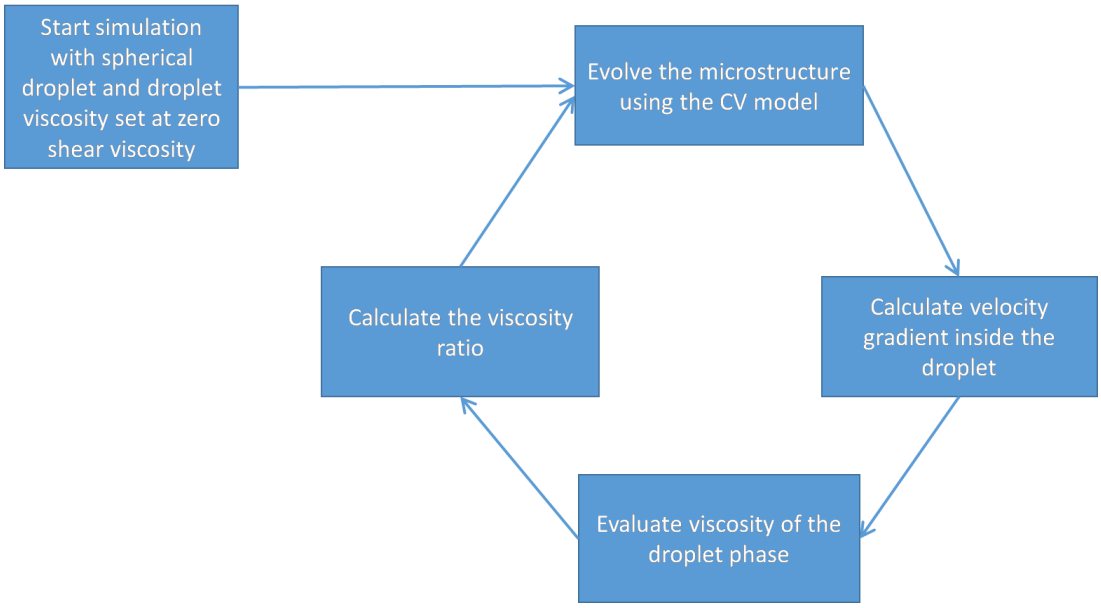

Figure 1: Schematic illustrating the cyclical dependence between droplet evolution and viscosity of droplet phase for a shear thinning droplet fluid.

the viscosity of the droplet shear-thinning fluid depends on the velocity gradient inside the droplet, the picture seems to indicate a cyclical dependence between the viscosity of the droplet phase and the velocity gradient inside the droplet. The idea is illustrated in Figure 1. Such a situation is very much amenable to a numerical solution. The modified constrained volume model is composed of coupled ordinary differential equations. In our numerical implementation, we use the fourth order-Runge Kutta method with a variable step-size and relative error acceptance criterion of less than 10^{-8}.

3 Results and Discussions

3.1 Fitting Flow Sweep Test Data of Boufarguine *et al.*

Figure 2 shows viscosity as a function of shear rate for a dense aqueous suspension of star-like micelles of poly(ethylene oxide) (PEO) hydrophobically end-capped with an octadecyl group that was used as droplet phase in the work of Boufarguine *et al.* [22]. The data are compared to predictions of the Carreau-Yasuda model [33], to predictions of the steady state Bautista *et al.* model and to the power law model. The Carreau-Yasuda model shows excellent agreement with the data using the parameters provided in Table 1. Note that the parameter η_o^* was given a very high value ($4{\cdot}10^8$ Pa·s) because there is no evidence in the experimental data of Boufarguine *et al.* of a plateau viscosity value at very low shear rate values. Moreover, the η_∞^* value was set to be the viscosity of water (0.001 Pa·s). The rest of the parameters were obtained through error minimization of a standard objective function. For a power law of the type $\eta^* = A * \dot{\gamma}^B$, the fit to the experimental data resulted in A = 493 Pa·s. and B = −0.806. This power law fit resulted in identical viscosity predictions as those obtained

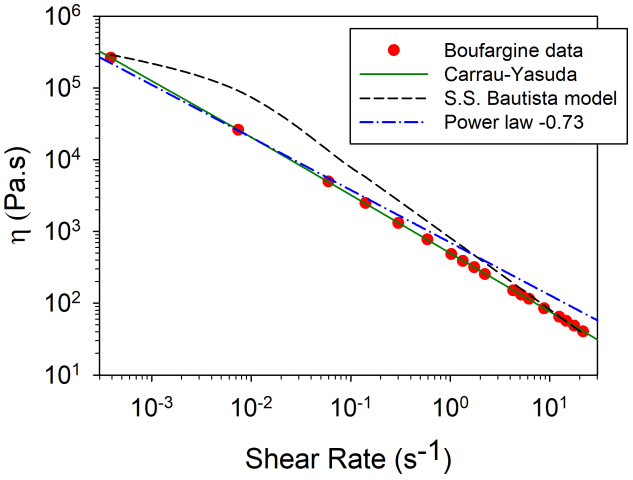

Figure 2: Experimental data of viscosity of polyoxyethylene water solution versus shear rate from Boufarguine *et al.* [22] compared to predictions using the Carreau-Yasuda model, the steady-state-Bautista *et al.* model and the power law model with exponent value of −0.73. Parameters of the Carreau-Yasuda model are provided in Table 1.

Table 1: Values of the Carreau-Yasuda model that were used in describing the experimental viscosity data of Boufarguine *et al.*

Parameter	Value
η_o^* (Pa·s)	$4.0{\cdot}10^{8.0}$
η_∞^* (Pa·s)	0.001
τ_{CY} (s)	$16.249{\cdot}10^{6}$
n	0.182
a	0.312
error (%)	0.26
R^2	0.999

by the Carreau-Yasuda model, and thus identical predictions of the shear thinning droplet deformation. Finally, we note here that there is an additional prediction denoted in the legend of the plot as power law with $B = -0.73$. This power law viscosity prediction curve will be revisited later.

For the Bautista Model in this part, we used the steady state viscosity (η_{ss}^*) solution of equation 7 and 8 as reported in [27] in the following form:

$$\frac{1}{\eta_{ss}^*} = \frac{1}{2}\left[-\left(k\tau_B\dot{\gamma}^{*2} - \frac{1}{\eta_o^*}\right) + \left(\left(k\tau_B\dot{\gamma}^{*2} - \frac{1}{\eta_o^*}\right)^2 + 4k\tau_B\dot{\gamma}^{*2}/\eta_\infty^*\right)^{\frac{1}{2}}\right] \tag{9}$$

The steady state viscosity of the Bautista *et al.* model was fit by specifying the value of the combined parameter $k\tau_B$. The fitting parameter value that can give reasonable results for subsequent plots was obtained by fitting the last part of the viscosity-shear rate data (*i.e.*, data at the higher end of the shear rate values). The value of the combined parameter $k\tau_B$ giving the best fit was $1.51{\cdot}10^{-9}$ s·Pa^{-1}, and η_∞^* is assumed to be the viscosity of water. Compared to the fit of Carreau-Yasuda, the Bautista *et al.* steady state viscosity predictions do not fit the experimental results as well as the Carreau-Yasuda fit does.

3.2 Comparison of CV Model Implementations to Experimental Data

We will compare in this part theoretical predictions to experimental results of a shear thinning droplet suspended in a Newtonian matrix provided by Boufarguine *et al.* However, since the droplet size was not explicitly stated in that paper, we use the data reported in Figures 10 and 11 of the Boufarguine *et al.* paper, and we assume that data points reported in those two figures have a droplet size that is the same as that used in producing other plots in the same paper. We found from our comparison of Figures 10 and 11 that droplet size is roughly around 150 mm for data where the viscosity of the matrix phase fluid was 30 Pa·s, and hence this value is used in all of our subsequent comparisons to the experimental data from that paper.

3.2.1 Comparison with Boufarguine *et al.* Data Under Shear Deformation

Figure 3 shows predictions of λ_{Lo} (droplet extension immediately after the stop of step-shear), compared to λ_{La}, which is the normalized droplet longest dimension after a given strain assuming affine flow as given by the following expression [22]:

$$\lambda_{La} = \frac{1}{2}\left(\gamma_o + \sqrt{4 + \gamma_o^2}\right) \tag{10}$$

where γ_o is the applied strain in a step-shear experiment. The experimental results were carried out at different applied shear rates. Part (a) of figure 3 shows a comparison to the original CV model, part (b) shows a comparison to the CV model combined with the Carreau-Yasuda model (CV-CY), part (c) shows a comparison to the CV-Bautista (CV-B) model and part (d) shows a comparison to the CV model combined with the power law model (CV-P). Figure 3-a was implemented by evaluating the viscosity of the droplet phase at external flow rate conditions. Figure 3-a demonstrates that the original CV model highly overestimates droplet deformation. On the other hand, Figures 3-b and 3c show similarity in trends with experimental data, but disagreement in values. The CV-B shows slightly better predictions than the CV-CY model. We note also that the CV-B model predictions start with a flat line as a consequence of droplet phase having a high viscosity value at the early stages of deformation. The values of A and B for the power law model are 700.0 Pa·s. and −0.73 respectively. The viscosity predictions of the power law model using those two parameters are shown in Figure 2. Note that the model predictions of the droplet behavior at applied shear rate of 16 s^{-1} agree with the experimental data only in the beginning of the step strain, then they diverge, where the model shows behavior akin to having an effective viscosity ratio value higher than 3.5, which is the condition necessary for a droplet to start showing tumbling behavior. In fact, if we calculate the apparent droplet viscosity according to the formula:

$$\frac{\lambda_{Lo} - 1}{\lambda_{La} - 1} = \frac{5}{2\,M + 3} \tag{11}$$

we find that the model is predicting an apparent droplet viscosity value of 296 Pa·s, giving an effective viscosity ratio value of 9.85.

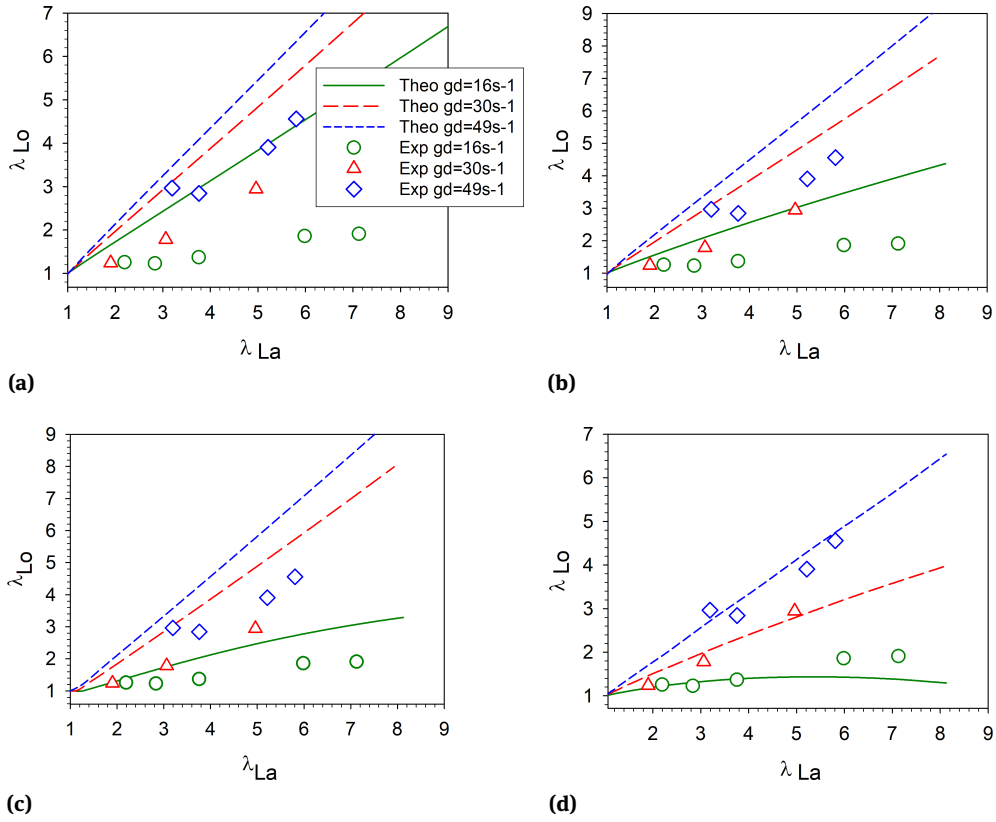

Figure 3: Stretching ratio after step shear carried out at specific shear rate values versus stretching ratio assuming affine deformation. Experimental data from Boufarguine *et al.* [22] are represented with circles for $\dot{\gamma} = 16\ s^{-1}$, triangles for $\dot{\gamma} = 30\ s^{-1}$, and diamond shapes for $\dot{\gamma} = 49\ s^{-1}$. Theoretical predictions using the CV model are represented by solid lines for $\dot{\gamma} = 16\ s^{-1}$, long dashes for $\dot{\gamma} = 30\ s^{-1}$ and short dashes for $\dot{\gamma} = 49\ s^{-1}$. In parts a, b, c and d, lines are predictions of the original CV model, the CV model combined with the Carreau-Yasuda shear thinning model, the CV model combined with the Bautista *et al.* model and the CV model combined with the power law with exponent value −0.73, respectively.

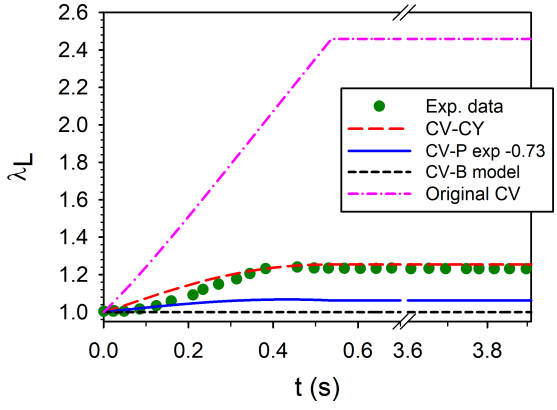

Figure 4: Normalized droplet length during and after a step shear experiment (from [22]) compared to the original CV, CV-CY, CV-B and CV-P models. In the experiment, the shear thinning droplet was subjected to step shear at 8 s^{-1} for 0.54 s, and then flow is stopped. The prediction curves show that the droplet does not retract after the shearing flow was stopped.

Figure 4 shows dimensionless droplet length versus time for a droplet subjected to shearing flow of 8 s^{-1}. The original CV model highly overestimates droplet deformation as in the previous figure. However, the CV-CY agrees with the experimental data very well, when compared to the CV-P, which highly underestimates the maximum that was observed experimentally. Lastly, the CV-B model does not show any deformation, because the viscosity of the droplet phase did not drop from its high zero-shear value during the step shear time.

3.2.2 Comparison with Delaby *et al.* Data Under Affine Extensional Deformation

A question can be raised about the accuracy of the constrained volume model itself in predicting droplet deformation as was shown in Figure 3. For that purpose, we compare the predictions of the model to the experimental

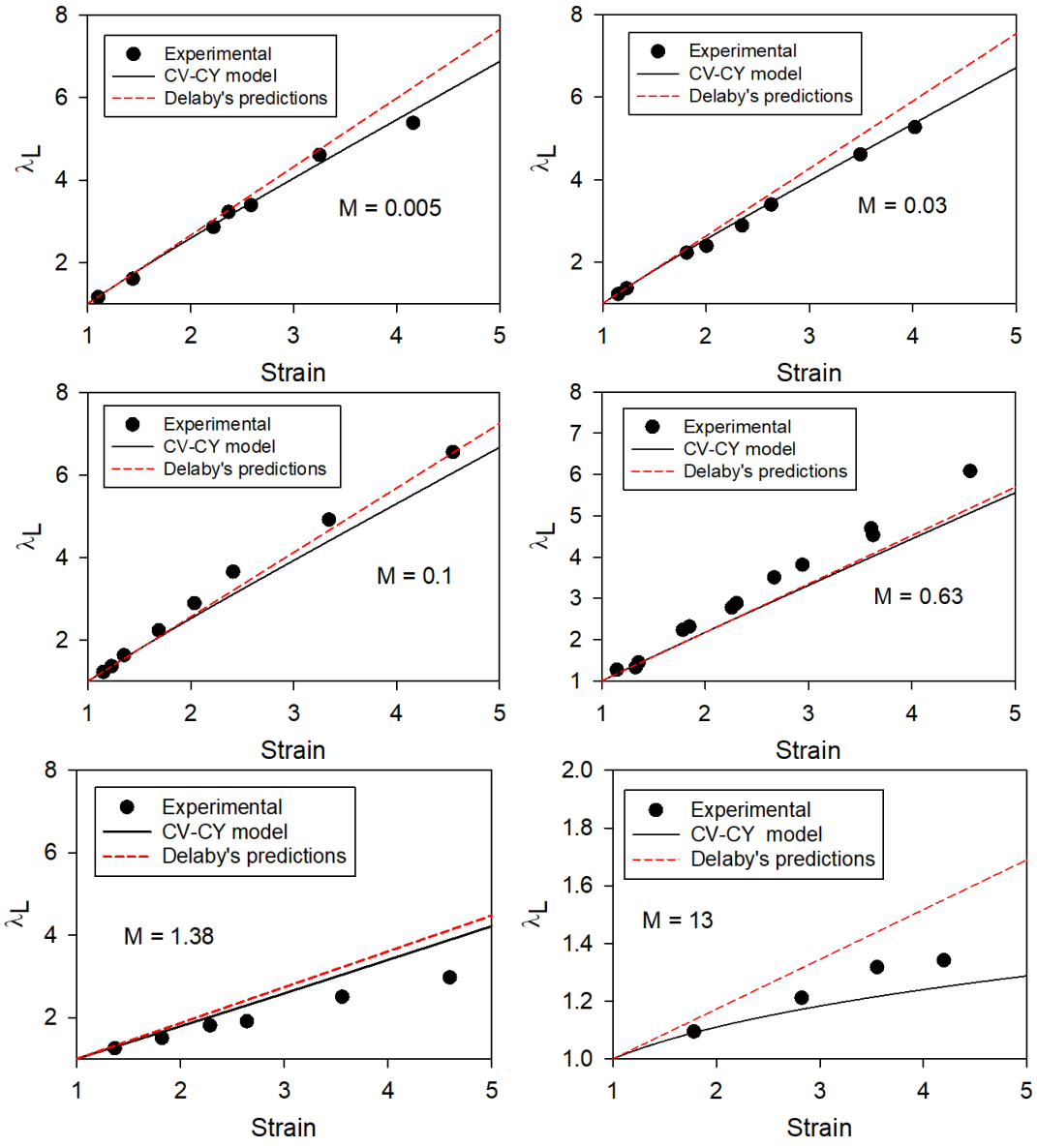

Figure 5: Stretching ratio (λ_L) versus applied strain during extensional flow. The experimental data are from Delaby *et al.* [21]. The figure compares the CV-CY model (solid lines) to the experimental data point as well as to predictions of Delaby *et al.* [21] (dashed lines). The corrected viscosity ratio value is displayed in each sub-figure. The blends are arranged from small to large viscosity ratio values, with blend components (major phase – minor phase) as follows: PS1-PE2, PS2-PE2, PS1-PE1, PS2-PE1, PS1-PMMA and PS2-PMMA. The viscosity of each component is obtained according to the Carreau-Yasuda parameters provided in Table 2.

Table 2: Values of the Carreau-Yasuda model for the polymers used in the Delaby *et al.* study [21].

Parameter	PS1	PS2	PE1	PE2	PMMA
η_o (Pa·s)	$3.00{\cdot}10^6$	$1.80{\cdot}10^5$	$1.6{\cdot}10^5$	$4.5{\cdot}10^3$	$2.8{\cdot}10^6$
η_∞ (Pa·s)	695.8	0.00	0.00	0.00	0.00
τ_{CY} (s)	34.26	3.852	11.249	0.288	61.264
n	0.0861	0.239	0.421	0.645	0.234
a	0.460	0.633	0.442	0.679	0.822

data of Delaby *et al.* [21], where non-Newtonian droplets are suspended in a non-Newtonian matrix. The experimental results of Delaby *et al.* are presented in a very similar way to the experimental results of Boufarguine *et al.* presented previously in Figure 3. The only difference is that while Boufarguine *et al.* carried out their experiments in a shearing flow, Delaby *et al.* carried out their experiments in an extensional flow for droplet and matrix fluids that are both shear thinning. Delaby *et al.* used polystyrene, polyethylene and polymethylmethacrylate as fluids for the matrix and droplet phases. Choices of matrix and droplet fluids were made in such a way that viscosity ratio values ranging from 0.005 to 13 could be obtained. The approach used by Delaby *et al.* was to calculate λ_{Lo} from the flow strength inside the droplet. For the case of extensional flow, flow strength inside the droplet is related to affine extension and droplet extension after step extension according to the following relation:

$$\frac{\lambda_{Lo}}{\lambda_{La}} = \frac{\exp\left(\dot{\epsilon}^{*} t\right)}{\exp\left(\dot{\epsilon} t\right)} \tag{12}$$

where $\dot{\epsilon}$ is the applied extensional rate and $\dot{\epsilon}^{*}$ is the extensional rate inside the droplet. This equation is coupled with Eq. 10 and equations describing the shear thinning behavior of both components to estimate the extensional rate inside the droplet and λ_{Lo}.

To model the deformation of droplets in the Delaby *et al.* study, their linear viscoelastic data of the shear thinning fluids was used together with the assumption of Cox-Merz rule to obtain the Carreau-Yasuda parameters for all the fluids that make up the blends. Note that it is not possible to use a power law to describe the viscosity data of the blends' components in the Delaby *et al.* study, as they all exhibit plateau viscosity, unlike the Boufarguine *et al.* data. We then run the CV-CY model at the conditions specified by the experiments of Delaby *et al.* with extensional rate of 0.01 s^{-1} and droplet diameter of 60 μm. The Carreau-Yasuda parameters for Delaby *et al.* fluids are provided in Table 2. The results of the comparison between the experimental data of Delaby *et al.* and the CV-CY model are shown in Figure 5. The figure shows predictions that are at least as good as the predictions made by Delaby *et al.* and are particularly better than those of Delaby *et al.* at small and large viscosity ratio values. There are no large disagreements with experimental data as was observed previously in Figure 3-b.

3.2.3 Comparison with Boufarguine *et al.* Relaxation Data After Step-Shear

Figure 6 shows experimental and theoretical predictions for droplet relaxation after step shear at different shear rate values (4 strain units with shear rate value of 16 s^{-1}, 6 strain units with shear rate value of 16 s^{-1}, and 4 strain units with shear rate value of 24 s^{-1}). The theoretical predictions of the CV-CY are generally close to the experimental behavior. However, the small relaxation observed experimentally is not observed theoretically. For the case of the CV-CY model, as soon as flow is stopped, the viscosity takes the value of the zero-shear rate viscosity, which makes it impossible for the droplet to relax. For the case of the CV-P with exponent value of −0.73, we see that the model vastly underestimates droplet deformation in all the comparisons to the step-shear experiments.

3.3 Overall Model Assessment in Describing Blends Composed of Shear Thinning Components

The overall evaluation of results of the comparisons with experimental data of Boufarguine *et al.* and Delaby *et al.* makes us lean towards the conclusion that the CV model coupled with a shear thinning description by a model such as the Carreau-Yasuda model is capable of satisfactorily describing experimental data of shear thinning droplet deformation. The CV-P with exponent value of −0.73 resulted in a good fit to Boufarguine's data in Figure 3-d due to the forced selection of the power law parameters. However, other comparisons to experimental data (c.f. Figures 4 and 6) using the exponent value of −0.73 resulted in poor agreement.

3.4 Improvement of the CV Model for the Case of Droplet Retraction

The decoupling approximation used in the CV model is the reason why the model does not display any retraction behavior when flow is stopped for a shear thinning droplet, although experimental data shows small relaxation followed by complete freezing of the flow. Thus, an estimation of the flow strength inside the droplet during relaxation is needed in order to calculate the viscosity of the retracting shear thinning droplet. Since the model is developed in terms of anisotropy rather than droplet dimensions, an expression was developed in terms of anisotropy invariants to describe droplet longest axis (L) based on the assumption of an axisymmetric prolate droplet. This expression is the

following:

$$L = 1.176 \times I_{\hat{q}}^{0.5} III_{\hat{q}}^{-0.5} \tag{13}$$

where $I_{\hat{q}}$ and $III_{\hat{q}}$ are the first and third invariants of anisotropy tensor, respectively. We assume that the speed of droplet retraction is equal to $\nabla v \cdot r$ [44], where r is a vector that represents the location of a point in space at the interface of the droplet. If we take r to be the point at the tip of the prolate droplet and that relaxation induces flow that can be approximated as the reverse of uniaxial extensional flow, then it follows that the velocity gradient tensor can be approximated as:

$$\nabla v = \begin{pmatrix} s & 0 & 0 \\ 0 & -0.5\,s & 0 \\ 0 & 0 & -0.5\,s \end{pmatrix} \tag{14}$$

where s, on dimensional grounds, can be estimated as $s \approx \frac{-c_1}{L}\frac{dL}{dt}$, and c_1 is introduced to the expression as a fitting constant. The value of the parameter c_1 was obtained by fitting the CV model to the experimental relaxation data displayed in Figure 6. The experimental droplet dimensions at the start of relaxation were used to calculate the anisotropy tensor components, which were used as the initial condition for the relaxation runs of the CV model. The experimental and theoretical droplet dimensions at the end of relaxation were used to calculate modeling error. Then, the error was minimized as a function of the fitting parameter c_1 and the best c_1 value was found. Figure 7 shows the results of this implementation, using $c_1 = 20.6$. At the end of the step shear and the start of retraction, the model shows minor change in droplet's dimensions taking place due to droplet retraction. As the driving force for droplet retrac-

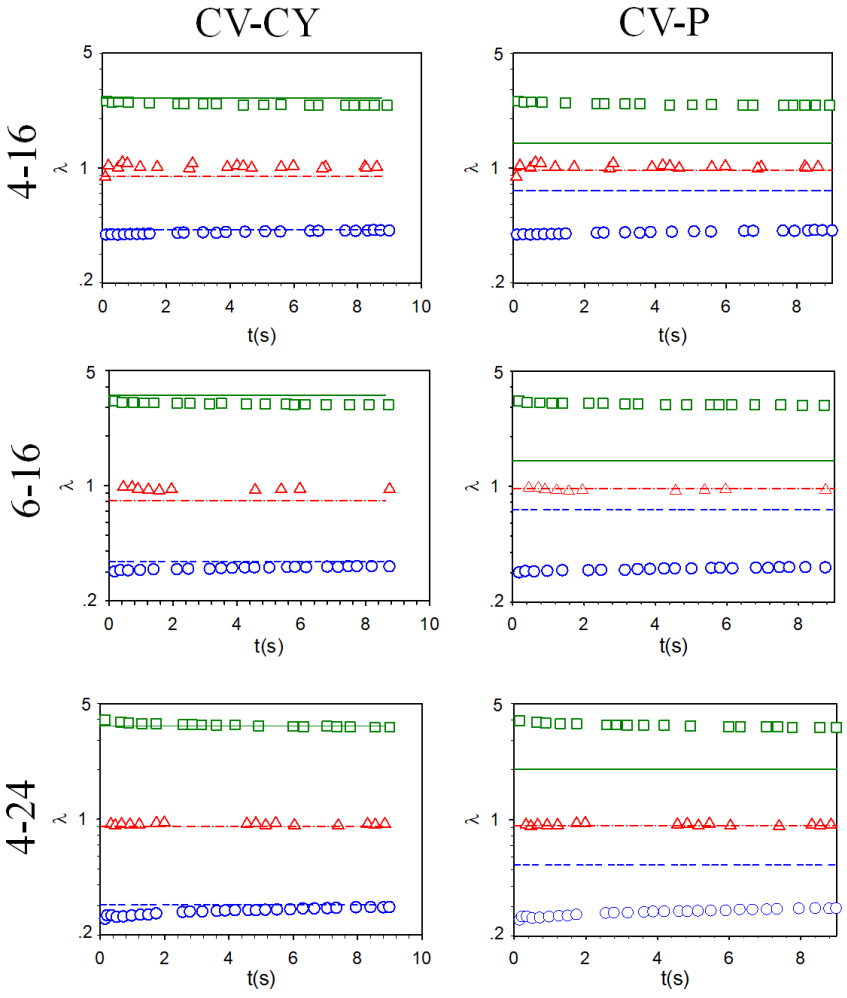

Figure 6: Normalized droplet dimensions as a function of time after step shear experiments (from [22]) carried out at different shear rates (row 1: strain = 4 and shear rate = 16 s^{-1} - denoted in the figure as 4-16, row 2: strain = 6 and shear rate = 16 s^{-1} - denoted as 6-16, and row 3: strain = 4 and shear rate = 24 s^{-1} - denoted as 4-24), compared to the CV-CY model (first column) and the CV-P model (second column). Squares, triangles and circles are experimental normalized droplet lengths, widths and thicknesses, respectively. Solid lines, dash-dotted lines and dashed lines are theoretical predictions using the CV model for normalized droplet lengths, widths and thicknesses, respectively.

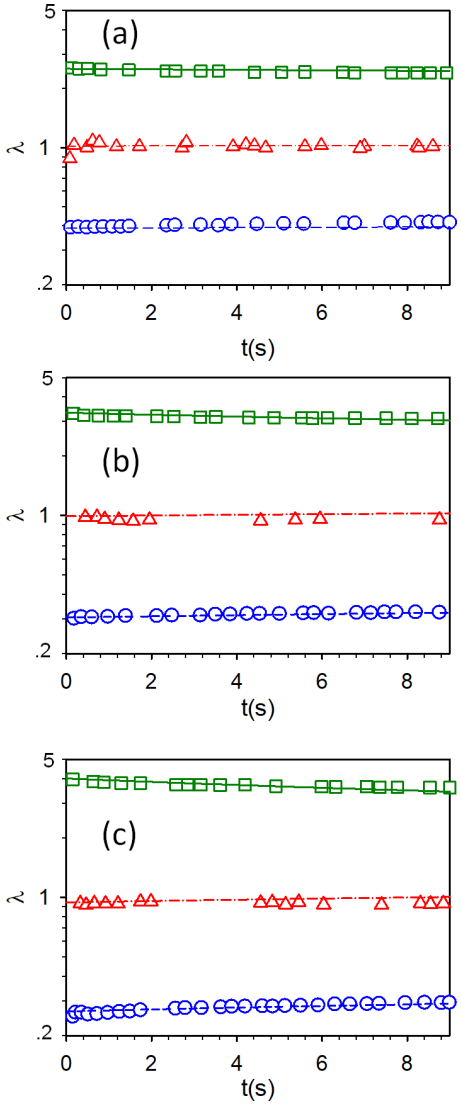

Figure 7: The same experimental data in Figure 6 are compared to the CV-CY model combined with approximate description of rate of deformation inside the droplet during droplet retraction. Parts a, b and c refer to strain value of 4 and shear rate value of 16 s^{-1}, strain value of 6 and shear rate value of 16 s^{-1} and strain value of 4 and shear rate value of 24 s^{-1}, respectively.

tion weakens due to the droplet becoming less extended, flow inside the droplet becomes slower and hence viscosity value of the fluid inside the droplet rises to the point where droplet dimensions practically cease from changing. The model shows excellent agreement with experimental data.

4 Conclusions

The constrained volume model was adapted to the case where a shear thinning droplet is suspended in a Newtonian fluid. Three approaches were suggested to describe the case. Only two approaches showed reasonable results: the constrained volume model combined with the Carreau-Yasuda model and the constrained volume model combined with the power law model. The third approach, the constrained volume model combined with Bautista *et al.* model, showed a failure in predicting the shear thinning viscosity behavior of the polyoxyethylene water solution of Boufarguine *et al.* and failed in describing droplet deformation during startup of shearing experiment. The simplicity of the power-law model makes it suitable for describing droplet deformation if it is composed of purely shear thinning fluid. On the other hand, the Carreau-Yasuda model has the advantage over the power-law model that it can describe viscosity data that has, or lacks, a plateau viscosity. The decoupling approximation, which is built in the approach of original Doi-Ohta model, implies that droplet retraction does not have any effect on internal flow. This issue was addressed by developing an expression for flow strength inside the droplet in terms of anisotropy invariants in such a way that the larger the droplet deformation, the larger the flow strength inside the droplet. By using this expression, the relaxation data of a shear thinning droplet was excellently described.

References

[1] Wetzel, E.D. and C.L. Tucker, *Droplet deformation in dispersions with unequal viscosities and zero interfacial tension*. J. Fluid Mech., 2001; **426**:199-228.
[2] Jackson, N.E. and C.L. Tucker, *A model for large deformation of an ellipsoidal droplet with interfacial tension*. J. Rheol., 2003; **47**:659-682.
[3] Almusallam, A.S., R.G. Larson, and M.J. Solomon, *A constitutive model for the prediction of ellipsoidal droplet shapes and stresses in immiscible blends*. J. Rheol., 2000 **44**:1055-1083.
[4] Almusallam, A.S., R.G. Larson, and M.J. Solomon, *Comprehensive constitutive model for immiscible blends of Newtonian polymers*. J. Rheol., 2004; **48**:319-348.
[5] Maffettone, P.L. and M. Minale, *Equation of change for ellipsoidal drops in viscous flow*. J. Non-Newtonian Fluid Mech., 1998; **78**:227-241.
[6] Peters, G.W.M., S. Hansen, and M.E.H. Meijer, *Constitutive modeling of dispersive mixtures*. J. Rheol., 2001; **45**:659-689.
[7] Yu, W. and M. Bousmina, *Ellipsoidal model for droplet deformation in emulsions*. J. Rheol., 2003; **47**(4):1011-1039.
[8] Wetzel, E.D. and C.L. Tucker, *Area tensors for modeling microstructures during laminar liquid-liquid mixing*. Int. J. Multiph. Flow, 1999; **25**:35-61.
[9] Greco, F., *Drop deformation for non-Newtonian fluids in slow flows*. Journal of Non-Newtonian Fluid Mechanics, 2002; **107**:111-131.
[10] Boger, D.V., *A highly elastic constant-viscosity fluid*. Journal of Non-Newtonian Fluid Mechanics, 1977; **3**(1):87-91.

[11] Maffettone, P.L. and F. Greco, *Ellipsoidal drop model for single drop dynamics with non-Newtonian fluids*. Journal of Rheology, 2004; **48**(1):83-100.
[12] Minale, M., *Deformation of a non-Newtonian ellipsoidal drop in a non-Newtonian matrix: extension of Maffettone-Minale model*. Journal of Non-Newtonian Fluid Mechanics, 2004; **123**(2-3):151-160.
[13] Yu, W., M. Bousmina, C.X. Zhou, and C.L. Tucker, *Theory for drop deformation in viscoelastic systems*. Journal of Rheology, 2004; **48**(2):417-438.
[14] Dressler, M. and B.J. Edwards, *The influence of matrix viscoelasticity on the rheology of polymer blends*. Rheol Acta, 2004; **43**:257-282.
[15] Dressler, M. and B.J. Edwards, *Rheology of polymer blends with matrix-phase viscoelasticity and a narrow droplet size distribution*. J. Non-Newtonian Fluid Mech., 2004; **120**:189-205.
[16] Yu, W., C. Zhou, and M. Bousmina, *Theory of morphology evolution in mixtures of viscoelastic immiscible components*. Journal of Rheology, 2005; **215**:215-236.
[17] Cardinaels, R., S. Afkhami, Y. Renardy, and P. Moldenaers, *An experimental and numerical investigation of the dynamics of microconfined droplets in systems with one viscoelastic phase*. Journal of Non-Newtonian Fluid Mechanics, 2011; **166**:52-62.
[18] Mukherjee, S. and K. Sarkar, *Effects of viscoelasticity on the retraction of a sheared drop*. Journal of Non-Newtonian Fluid Mechanics, 2010; **165**(7-8):340-349.
[19] Gupta, A. and M. Sbragaglia, *Deformation and break-up of viscoelastic droplets in confined shear flow*. Phys. Rev. E.; **90**:023305.
[20] Elmendorp, J. and R. Maalcke, *A study on polymer blending microrheology: Part 1*. Polymer Engineering & Science, 1985; **25**(16):1041-1047.
[21] Delaby, I., B. Ernst, Y. Germain, and R. Muller, *Droplet deformation in polymer blends during uniaxial elongational flow: Influence of viscosity ratio for large capillary numbers*. Journal of Rheology, 1994; **38**:1705-1720.
[22] Boufarguine, M., F. Renou, T. Nicolai, and L. Benyahia, *Droplet deformation of a strongly shear thinning dense suspension of polymeric micelles*. Rheologica Acta, 2010; **49**(6):647-655.
[23] Favelukis, M., O.M. Lavrenteva, and A. Nir, *Deformation and breakup of a non-Newtonian slender drop in an extensional flow*. Journal of Non-Newtonian Fluid Mechanics, 2005; **125**:49-59.
[24] Harvie, D.J.E., M.R. Davidson, C.-W. J.J., and M. Rudman, *A parametric study of droplet deformation through a microfluidic contraction: Shear thinning liquids*. Int. J. Multiph. Flow, 2007; **33**:545-556.
[25] Giraldo, M., H. Power, and W.F. Florez, *Numerical simulation of the motion and deformation of a non-Newtonian shear-thinning drop suspended in a Newtonian circular Couette flow using DR-BEM*. Engineering Analysis with Boundary Elements, 2009; **33**:93-104.
[26] Tyagi, S., A.K. Ghosh, P. Montanari, G.W.M. Peters, and H.E.H. Meijer, *Linear Viscoelastic and Transient Behavior of Polypropylene and Ethylene Vinyl Acetate Blends: An Evaluation of the Linear Palierne and a Nonlinear Viscoelastic Model for Dispersive Mixtures*. Polymer engineering and science, 2002; **42**(11):2107-2119.
[27] Bautista, F., J.M. de Santos, J.E. Puig, and O. Manero, *Understanding thixotropic and antithixotropic behavior of viscoelastic micellar solutions and liquid crystalline dispersions. I. The model*. Journal of Non-Newtonian Fluid Mechanics, 1999; **80**(2-3):93-113.
[28] Wetzel, E.D., *Modeling flow-induced microstructure in inhomogeneous liquid-liquid mixtrures.*, in *Mechanical Engineering*. 1999, University of Illinois: Urbana-Champaign.
[29] Almusallam, A.S., *The modified constrained volume model predictions in shearing flow at nonunity viscosity ratio values*. Rheol Acta, 2013; **52**(6):607-621.
[30] Doi, M. and T. Ohta, *Dynamics and rheology of complex interfaces. I* J. Chem. Phys., 1991; **95**:1242-1248.
[31] Almusallam, A.S., *Large Amplitude Oscillatory Shear of Immiscible Polymer Blends and Comparison to Anisotropy and Droplet Models*. J. Rheol., 2014; **58**:1903-1916.
[32] Cates, M.E. and S.M. Fielding, *Rheology of giant micelles*. Advances in Physics, 2006; **55**(7-8):799-879.
[33] Macosko, C.W., *Rheology: Principles, Measurements, and Applications*. First Edition ed. 1994: Wiley-VCH.
[34] Olmsted, P.D., O. Radulescu, and C.Y.D. Lu, *Johnson-Segalman model with a diffusion term in cylindrical Couette flow*. Journal of Rheology, 2000; **44**(2):257-275.
[35] Vasquez, P.A., G.H. McKinley, and L.P. Cook, *A network scission model for wormlike micellar solutions - I. Model formulation and viscometric flow predictions*. Journal of Non-Newtonian Fluid Mechanics, 2007; **144**(2-3):122-139.
[36] Larson, R.G., *Constitutive equations for thixotropic fluids*. Journal of Rheology, 2015; **59**(3):595-611.
[37] Manero, O., F. Bautista, J.F.A. Soltero, and J.E. Puig, *Dynamics of worm-like micelles: the Cox-Merz rule*. Journal of Non-Newtonian Fluid Mechanics, 2002; **106**(1):1-15.
[38] Boek, E.S., J.T. Padding, V.J. Anderson, P.M.J. Tardy, J.P. Crawshawa, and J.R.A. Pearson, *Constitutive equations for extensional flow of wormlike micelles: stability analysis of the Bautista–Manero model*. J. Non-Newtonian Fluid Mech., 2005; **126**:39-46.
[39] Yamamoto, T., T. Hashimoto, and A. Yamashita, *Flow analysis for wormlike micellar solutions in an axisymmetric capillary channel*. Rheologica Acta, 2008; **47**(9):963-974.
[40] Yamashita, A., T. Yamamoto, and T. Hashimoto, *Numerical Simulation of Startup Flows of Wormlike Micellar Solutions in an Axisymmetric Capillary Channel using a Modified Bautista-Manero Model*. Nihon Reoroji Gakkaishi, 2009; **37**(2):69-74.
[41] Fredrickson, A.G., *A model for the thixotropy of suspensions*. AIChE Journal, 1970; **16**(3):436-441.
[42] Stephanou, P.S. and G.G. Georgiou, *A nonequilibrium thermodynamics perspective of thixotropy*. The Journal of Chemical Physics, 2018; **149**(24):244902.
[43] Stephanou, P.S., *A constitutive hemorheological model addressing both the deformability and aggregation of red blood cells*. Physics of Fluids, 2020; **32**(10):103103.
[44] Fuller, G.G., *I. Dynamics of flowing polymer solutions. II. The measurement of velocity gradients by homodyne light scattering spectroscopy*. 1980, California Institute of Technology.

A Calculation of Average Velocity Gradient Tensor Inside the Droplet

The procedure for obtaining the average velocity gradient inside the droplet from the anisotropy tensor, the imposed velocity gradient tensor and viscosity ratio is as follows [28]:

1. Obtain the area tensor from the anisotropy tensor, where the area tensor is defined as:

$$A_{\alpha\beta} = \hat{q}_{\alpha\beta}/I_{\hat{q}} \tag{A1}$$

2. Obtain the eigenvalues of the $A_{\alpha\beta}$ tensor and arrange them in decreasing order. Save the order of arrangement.
3. It is necessary to obtain the fourth order tensor S. The S tensor has five basic components that can be related to the arranged eigenvalues of the area tensor as follows:

$$\begin{aligned} S_1 = (&4.17625039658827 \\ &- 9.20850661941592A_1 \\ &- 0.553135609689901A_1^2 \\ &+ 21.6874206451302A_1^3 \\ &- 21.2568710422144A_1^4 \\ &+ 6.1548422296018A_1^5 \\ &- 42.616540944532A_2 \\ &+ 113.829950489808A_1A_2 \\ &- 86.7500411371294A_1^2A_2 \\ &+ 0.365874036598785A_1^3A_2 \\ &+ 15.1417807406092A_1^4A_2 \\ &+ 153.020181943596A_2^2 \\ &- 343.813953201013A_1A_2^2 \\ &+ 241.125657171276A_1^2A_2^2 \\ &- 49.4898901316211A_1^3A_2^2 \\ &- 257.958946460697A_2^3 \\ &+ 395.622455351456A_1A_2^3 \\ &- 145.078706965184A_1^2A_2^3 \\ &+ 215.596803577334A_2^4 \\ &- 168.449082343817A_1A_2^4 \\ &-70.6599267550296A_2^5\Big)^2 \end{aligned} \tag{A2}$$

$$\begin{aligned} S_2 = (&4.17625039658827 \\ &- 34.2616658055224A_1 \\ &+ 94.3983307383786A_1^2 \\ &- 119.36024295102A_1^3 \\ &+ 71.4515933564552A_1^4 \\ &- 16.4042657348787A_1^5 \\ &- 17.5633817584255A_2 \\ &+ 153.060848346559A_1A_2 \\ &- 344.370272249619A_1^2A_2 \\ &+ 303.717692700773A_1^3A_2 \\ &- 93.5896810636499A_1^4A_2 \\ &+ 18.8378177387772A_2^2 \\ &- 230.603225189622A_1A_2^2 \\ &+ 398.946506608063A_1^2A_2^2 \\ &- 184.220910397017A_1^3A_2^2 \\ &+ 27.5982202365534A_2^3 \\ &+ 122.691400831295A_1A_2^3 \\ &- 151.841781877225A_1^2A_2^3 \\ &- 65.3532744021372A_2^4 \\ &+ 2.72925202332791A_1A_2^4 \\ &+30.9464032180017A_2^5\Big)^2 \end{aligned} \tag{A3}$$

$$\begin{aligned} S_3 = (&-40.7723330492405 \\ &+ 225.30698049376A_1 \\ &- 510.579507296145A_1^2 \\ &+ 597.728209754151A_1^3 \\ &- 360.307571512262A_1^4 \\ &+ 88.6242216097376A_1^5 \\ &+ 310.483574745563A_2 \\ &- 1308.24247156398A_1A_2 \\ &+ 2146.12778534329A_1^2A_2 \\ &- 1629.00562122183A_1^3A_2 \\ &+ 479.860149860514A_1^4A_2 \\ &- 934.211287968719A_2^2 \\ &+ 2868.24184948991A_1A_2^2 \\ &- 3050.03472285699A_1^2A_2^2 \\ &+ 1125.43908724485A_1^3A_2^2 \\ &+ 1403.22822221236A_2^3 \\ &- 2816.03840013891A_1A_2^3 \\ &+ 1461.76816239862A_1^2A_2^3 \\ &- 1049.55576568688A_2^4 \\ &+ 1038.39259315147A_1A_2^4 \\ &+310.827589746918A_2^5\Big)^2 \end{aligned} \tag{A4}$$

$$
\begin{aligned}
S_4 = (&0.582186603041814 \\
&- 1.77064557477319A_1 \\
&+ 3.21220714043462A_1^2 \\
&- 2.77788406828005A_1^3 \\
&+ 0.17708298096669A_1^4 \\
&+ 0.577052918610156A_1^5 \\
&- 1.668651593392 46A_2 \\
&+ 4.81231528227066A_1A_2 \\
&- 13.1653042138577A_1^2A_2 \\
&+ 13.5960292792509A_1^3A_2 \\
&- 3.660675836098 19A_1^4A_2 \\
&+ 0.331554784838164A_2^2 \\
&+ 2.60424478697637A_1A_2^2 \\
&+ 8.26789627322757A_1^2A_2^2 \\
&- 8.288186504622 54A_1^3A_2^2 \\
&+ 1.803196776492 29A_2^3 \\
&- 13.4975620028569A_1A_2^3 \\
&+ 4.012091480310 42A_1^2A_2^3 \\
&+ 0.802756308377304A_2^4 \\
&+ 6.211506250867 56A_1A_2^4 \\
&-1.85104297935 71A_2^5\Big)^2
\end{aligned}
\tag{A5}
$$

$$
\begin{aligned}
S_5 = (&0.464027821843141 \\
&- 2.620300995783 52A_1 \\
&+ 6.048061722375 24A_1^2 \\
&- 7.093891133431 62A_1^3 \\
&+ 4.204960581365 89A_1^4 \\
&- 1.002857996369 13A_1^5 \\
&- 3.138037622432 91A_2 \\
&+ 13.59295833916 71A_1A_2 \\
&- 22.57791366665A_1^2A_2 \\
&+ 16.99307456058 35A_1^3A_2 \\
&- 4.870738831897 19A_1^4A_2 \\
&+ 9.947535141092 64A_2^2 \\
&- 30.53322949489 41A_1A_2^2 \\
&+ 32.56441375627 49A_1^2A_2^2 \\
&- 11.90515082599 64A_1^3A_2^2 \\
&- 13.88780127765 87A_2^3 \\
&+ 28.79060853641 73A_1A_2^3 \\
&- 15.14128832949 6A_1^2A_2^3 \\
&+ 9.830711353630 56A_2^4 \\
&- 10.24375946136 84A_1A_2^4 \\
&-2.656313869477 35A_2^5\Big)^2
\end{aligned}
\tag{A6}
$$

4. We then calculate the components of the fourth order Eshelby tensor S in contracted notation (6×6 matrix) as follows:

$$S_{33} = S_1 \tag{A7}$$

$$S_{22} = S_2 \tag{A8}$$

$$S_{11} = S_3 \tag{A9}$$

$$S_{12} = S_4 \tag{A10}$$

$$S_{23} = S_5 \tag{A11}$$

$$S_{13} = 1 - S_{23} - S_{33} \tag{A12}$$

$$S_{32} = 1 - S_{12} - S_{22} \tag{A13}$$

$$S_{44} = 0.5\,(S_{23} - S_{32}) \tag{A14}$$

$$S_{21} = \frac{(3 - S_{11} - S_{22} - S_{33})}{2} - S_{32} - S_{13} \tag{A15}$$

$$S_{66} = 0.5\,(S_{21} + S_{12}) \tag{A16}$$

$$S_{31} = 1 - S_{11} - S_{21} \tag{A17}$$

$$S_{55} = 0.5\,(S_{31} + S_{13}) \tag{A18}$$

The other components of the fourth order S tensor in contracted notation have zero values.

5. We calculate the components of the fourth order alternate Eshelby tensor T as follows:

$$T_{44} = 0.5\,(S_{32} - S_{23}) \tag{A19}$$

$$T_{55} = 0.5\,(S_{13} - S_{31}) \tag{A20}$$

$$T_{66} = 0.5\,(S_{21} - S_{12}) \tag{A21}$$

The other components of the fourth order alternate Eshelby tensor T in contracted notation have zero values.

6. Obtain the value of the D_b parameter as follows:

$$\nu = M - 1 \tag{A22}$$

$$\begin{aligned} D_b = {} & 1 + \nu\,(S_{11} + S_{22} + S_{33}) \\ & + \nu^2\,(S_{11}S_{22} + S_{22}S_{33} + S_{33}S_{11} - S_{12}S_{21} \\ & - S_{23}S_{32} - S_{31}S_{13}) + \nu^3\,(S_{11}S_{22}S_{33} + S_{12}S_{23}S_{31} \\ & + S_{21}S_{32}S_{13} - S_{11}S_{23}S_{32} - S_{22}S_{31}S_{13} \\ & - S_{33}S_{12}S_{21}) \end{aligned} \tag{A23}$$

7. Obtain the fourth order concentration tensor Btensor in contracted notation as follows:

$$B_{11} = \frac{\left[1 + \nu\,(S_{22} + S_{33}) + \nu^2\,(S_{22}S_{33} - S_{23}\,S_{32})\right]}{D_b} \tag{A24}$$

$$B_{22} = \frac{\left[1 + \nu\,(S_{33} + S_{11}) + \nu^2\,(S_{33}S_{11} - S_{31}S_{13})\right]}{D_b} \tag{A25}$$

$$B_{33} = \frac{\left[1 + \nu\,(S_{11} + S_{22}) + \nu^2\,(S_{11}S_{22} - S_{12}S_{21})\right]}{D_b} \tag{A26}$$

$$B_{12} = -\nu\frac{[S_{12} + \nu\,(S_{12}S_{33} - S_{13}S_{32})]}{D_b} \tag{A27}$$

$$B_{21} = -\nu\frac{[S_{21} + \nu\,(S_{21}S_{33} - S_{23}S_{31})]}{D_b} \tag{A28}$$

$$B_{23} = -\nu\frac{[S_{23} + \nu\,(S_{23}S_{11} - S_{21}S_{13})]}{D_b} \tag{A29}$$

$$B_{32} = -\nu\frac{[S_{32} + \nu\,(S_{32}S_{11} - S_{31}S_{12})]}{D_b} \tag{A30}$$

$$B_{31} = -\nu\frac{[S_{31} + \nu\,(S_{31}S_{22} - S_{32}S_{21})]}{D_b} \tag{A31}$$

$$B_{13} = -\nu\frac{[S_{13} + \nu\,(S_{13}S_{22} - S_{12}S_{23})]}{D_b} \tag{A32}$$

$$B_{44} = \frac{1}{(2 + 4\nu S_{44})} \tag{A33}$$

$$B_{55} = \frac{1}{(2 + 4\nu S_{55})} \tag{A34}$$

$$B_{66} = \frac{1}{(2 + 4\nu S_{66})} \tag{A35}$$

The other components of the fourth order B tensor in contracted notation have zero values.

8. Obtain the fourth order concentration tensor C as follows:

$$C_{44} = -\nu\frac{T_{44}}{(1 + 2\nu S_{44})} \tag{A36}$$

$$C_{55} = -\nu\frac{T_{55}}{(1 + 2\nu S_{55})} \tag{A37}$$

$$C_{66} = -\nu\frac{T_{66}}{(1 + 2\nu S_{66})} \tag{A38}$$

9. Construct the fourth order concentration tensors B and C using:

$$B_{RT(i,1),RT(i,1),\ RT(j,1),\ RT(j,1)} = B_{ij}, \quad i = 1..3, j = 1..3. \tag{A39}$$

$$B_{RT(i,1),RT(i,2),\ RT(j,1),\ RT(j,2)} = B_{ij}, \quad i = 4..6, j = 4..6. \tag{A40}$$

$$B_{RT(i,1),RT(i,2),\ RT(j,2),\ RT(j,1)} = B_{ij}, \quad i = 4..6, j = 4..6. \tag{A41}$$

$$B_{RT(i,2),RT(i,1),\ RT(j,2),\ RT(j,1)} = B_{ij}, \quad i = 4..6, j = 4..6. \tag{A42}$$

$$C_{RT(j,1),RT(j,1),\ RT(i,1),\ RT(i,1)} = C_{ij}, \quad i = 1..3, j = 1..3. \tag{A43}$$

$$C_{RT(i,1),RT(i,2),\ RT(j,1),\ RT(j,2)} = C_{ij}, \quad i = 4..6, j = 4..6. \tag{A44}$$

$$C_{RT(i,2),RT(i,1),\ RT(j,1),\ RT(j,2)} = -C_{ij}, \quad i = 4..6, j = 4..6. \tag{A45}$$

$$C_{RT(i,1),RT(i,2),\ RT(j,2),\ RT(j,1)} = C_{ij}, \quad i = 4..6, j = 4..6. \tag{A46}$$

$$C_{RT(i,2),RT(i,1),\ RT(j,2),\ RT(j,1)} = -C_{ij}, \quad i = 4..6, j = 4..6. \tag{A47}$$

RT denotes the reconstruction table provided in Table A1

10. Rearrange the fourth order concentration tensor according to the saved order of arrangement in step 2.
11. Rotate $E_{\alpha\beta}$ and $\Omega_{\alpha\beta}$ to the droplet eigen frame.
12. Calculate the velocity gradient inside the droplet $\kappa^{\star}_{\alpha\beta}$ in the eigen frame according to Eq. 1.
13. Rotate $\kappa^{\star}_{\alpha\beta}$ back to the original frame.

Table A1: Reconstruction table containing indices that relate fourth order tensors (B and C) in contracted notation to their expanded form.

First index	Second index
1	1
2	2
3	3
2	3
3	1
1	2